APPENDIX

Table of Contents:

Appendix Supplementary Methods

Plasmids and antibodies

With the exception of the mouse RBPJ missense mutants [Fig 2; previously described in (Yuan *et al*, 2012)], the mouse GST-RBPJ fusion [Appendix Fig S1C and D; previously described in (Liefke *et al*, 2010)], the mouse RBPJ-(53-474) core domain [Fig 3A; previously described in (Collins *et al*, 2014); accession #P31266.1], the mouse NOTCH1 ICD ΔOP [Appendix Fig S1C and D; previously described in (Oswald *et al*, 2001)], the mouse NOTCH1 ICD ΔOP [Appendix Fig S5B and C; previously described in (Jung *et al*, 2013)] and the *Drosophila* constructs, all the plasmids used in this study express human proteins. The protein-encoding Open Reading Frames (ORFs) of RBPJ (accession #KJ897041), L3MBTL3 (accession #KJ899798) and KDM1A (accession #EL734007) cloned as Gateway® Entry clones were obtained from the Center for Cancer Systems Biology (CCSB, Harvard Medical School, Boston, USA) human ORFeome collection or were cloned by Gateway® recombination cloning from cDNA plasmids as previously described (Rual *et al*, 2004, Yang *et al*, 2011). The NOTCH1 ICD cDNA clone used for Gateway® sub-cloning was a generous gift of Dr. W. Pear (University of Pennsylvania,

USA). The RBPJ and L3MBTL3 deletion mutants were generated by site-directed mutagenesis from RBPJ and L3MBTL3 Gateway® Entry clones. The pGEX6P1-Su(H) construct used in Fig 6A was previously described (Liefke *et al*, 2010). The pRmHA-3-dL(3)mbt was a generous gift of I. Macinkovic and Dr. A. Brehm (University of Marburg, Germany). The Y2H pDEST-DB and pDEST-AD vectors as well as the p-DEST-MYC Gateway® destination vector were generously provided by the CCSB. The pcDNA3-HA-DEST protein expression vector was kindly provided by Dr. S. Li (University of Michigan, Ann Arbor, USA). The pBABE-SFB (S-FLAG-SBP triple tag) vector was provided by Dr. J. Huang (Zhejiang University, China). The MigR1 vector and DN-MAML (Maillard *et al*, 2004) plasmids were kindly provided by Dr. I. Maillard (University of Michigan, Ann Arbor, USA). The following vectors were obtained from Addgene®: pLIX402, a doxycycline inducible lentiviral Gateway® destination vector; pLX304, a V5 epitope tag lentiviral Gateway® destination vector; and lentiCRISPR-EGFP-sgRNA1, a CRISPR/Cas9 genome editing vector. The pcDNA 3.1 Flag2 (Invitrogen®) and pGEX6P1 (GE Healthcare®) were commercially acquired. The pcDNA3.1 HA-hL3MBTL3, pcDNA3.1 HA-hL3MBTL3 NTD, pcDNA3.1 HA-hL3MBTL3 CTD, pcDNA3.1 FLAG-dL(3)mbt and pcDNA3.1 FLAG-dmNICD, containing the RAM domain and ANK repeats, were cloned via PCR in pSC-A-amp/kan (Agilent Technologies®, 240205-5) or pJET (Thermo Scientific®, K1232), digested with the desired restriction enzymes (New England Biolabs®), cloned into the destination vectors and sequence-verified by DNA sequencing. The sh-*RBPJ* and sh-*L3MBTL3* constructs used in Fig 4 and Appendix Fig S3 and S4 were obtained from Open Biosystems® [Oligo ID #: V2LHS-263385 (RBPJ) and V2LHS-100673 (L3MBTL3)]. The sh-*L3mbtl3* constructs #1 and #2 used in Appendix Fig S5 were obtained from the pLK0.1 Harvard shRNA library. The target sequences of the hairpins and all oligonucleotides used in this study are listed in Table EV2.

The following primary antibodies were used: L3MBTL3 [Bethyl®, A302-852A (Western blotting) and A302-854A (ChIP)], RBPJ [Cell Signaling®, 5313 (Western blotting) and Santa Cruz® sc-

271128 (IP)], KDM1A (Cell Signaling®,2184), *Drosophila* dNICD [9C6, 1:500] (Fehon *et al*, 1990), *Drosophila* elav (Developmental Studies Hybridoma Bank, 7E8A10), *Drosophila* cut (Developmental Studies Hybridoma Bank, 2B10), H3K4me2 (Cell Signaling®, 9725), Dlg (Developmental Studies Hybridoma Bank, 4F3), Dpn (Weng *et al*, 2010), HA [Roche®, 12013819001 (Western blotting); Abcam®, ab9110 (ChIP); Roche® 11867423001 (*Drosophila,* IF)], FLAG (Sigma®, A8592), MYC (Roche®, 11814150001), V5 [Thermo Scientific®, MA5-15253 (Western blotting); Sigma®, A7345 (ChIP)], RNAPII (Santa Cruz®, sc-899), GAPDH (Abcam®, ab8245), cleaved NOTCH1 (Val1744; Cell Signaling®, 2421) and β-actin (Cell Signaling®, 5125). Secondary antibodies were purchased from Cell Signaling® (goat α-rabbit IgG, 7074 and horse α-mouse IgG, 7076). For the detection of Bio-tagged NOTCH1 ICD ΔOP, streptavidin-HRP conjugate (Perkin-Elmer®, NEL750001EA) was used.

Cell lines and cell culture conditions

The U87-MG, MDA-MB-231 and HEK293T cell lines were obtained from Drs. Y. Sun, C. Kleer and X. Yu, respectively (University of Michigan, Ann Arbor, USA). U87-MG, HEK293T and *Phoenix*™ packaging (Orbigen®) cells were cultivated in DMEM medium supplemented with 10% FBS and penicillin/streptomycin. MDA-MB-231 cells were cultivated in RPMI1640 medium supplemented with 10% FBS and penicillin/streptomycin. The cells used in Appendix Fig S5 are a clonal mouse hybridoma mature T-cell line and a mouse pre-T cell line called Beko (Oswald *et al*, 2016) and were grown in Iscove's Modified Dulbecco Medium (IMDM, Gibco®) supplemented with 2% FCS, 0.3 mg l^{-1} peptone, 5 mg l^{-1} insulin, nonessential amino acids and penicillin/streptomycin. Protein expression, shRNA and CRISPR/Cas9 vectors were transfected into cells using polyethylenimine (Polysciences®, 23966-2) as previously described (Longo *et al*, 2013) or by lentiviral/retroviral infection using standard protocols. *Phoenix*™ packaging cells were transfected using the calcium phosphate method. Selection of positively infected clones was obtained with puromycin (2 μg ml^{-1}; Sigma®, P8833), histidinol (500 μM; Sigma®, H6647) or

blasticidin (10 µg ml^{-1}; Invitrogen®, R210-01). For the γ-secretase inhibitor (GSI) experiments, U87-MG and MDA-B-231 cells were treated with 1 µM DBZ (Calbiochem®, 209984-56-5) for 48 h. Cell line authentications were performed by STR profiling. Cell lines have been tested for mycoplasma contamination.

Protein immuno-precipitation in U87-MG and HEK293T cells

U87-MG, MDA-MB-231 and HEK293T cells were harvested and lysed at 4°C for 30 min in lysis buffer [50 mM Tris pH 7.8, 150 mM NaCl, 0.5% NP-40, 10% glycerol, 2 mM NaF, 2 mM Na_3VO_4, and Complete® protease inhibitor (1X final, Roche®, 05 056 489 001)]. Cell lysates were cleared by centrifugation for 10 minutes at 21100 g and protein extracts were incubated with 30 µl of the desired resin (α-HA agarose, Sigma®, A2095; α-FLAG agarose, Sigma®, A2220; streptavidin agarose, Thermo Scientific®, 20361; α-V5 agarose, Sigma®, A7345; α-RBPJ agarose, Santa Cruz®, sc-271128 AC) at 4°C for 3 hours. Beads were washed four times with lysis buffer and proteins were eluted by boiling for five minutes in Laemmli sample buffer. Proteins were resolved via SDS-PAGE and analyzed via Western blotting using standard immuno-blotting techniques. The competition IP assays (Fig 3B and C) were performed using the same approach. All the immuno-precipitation experiments were replicated at least twice and representative results are shown in the figures.

Nuclear or whole cell extraction from mature T-cells and pre-T cells

Nuclear extract from mature T-cells was prepared as follows: cells were washed twice with PBS (Gibco®) and resuspended in ice cold hypotonic buffer (20 mM Hepes pH 7.9, 20 mM NaCl, 5 mM $MgCl_2$, 10% glycerol, 0.2 mM PMSF) at the concentration of 10 x 10^6 cells ml^{-1}. After 20 minutes incubation on ice, the cell suspension was vortexed 20 seconds and centrifuged five minutes at 14000 rpm at 4°C. Nuclei were washed in PBS and resuspended in hypertonic buffer [20 mM Hepes pH 7.9, 300 mM NaCl, 1 mM $MgCl_2$, 0.2 % NP-40, 25% glycerol, 0.3 mM

Dithiothreitol (DTT), 1 x protease inhibitor mix (Roche® 05056489001) and 0.2 mM PMSF] at the concentration of 10000 cells μl^{-1}. After 20 minutes incubation on ice, the lysate was cleared by centrifugation at 14000 rpm for five minutes at 4°C.

Whole cell extracts from mature T-cells and pre-T cells (Beko) were prepared as follows: cells were washed twice with PBS (Gibco®) and resuspended in ice cold whole cell extraction buffer [20 mM Tris-HCl pH 8.0, 150 mM NaCl, 1% NP-40, 10% glycerol, 0.5 mM Na_3VO_4, 10 mM NaF, 1 mM PMSF, 1x proteinase inhibitor cocktail (Roche® 05056489001)]. After 20 min incubation on ice, the cell suspension was centrifuged 15 min at 13200 rpm at 4°C and the supernatant was recovered. Protein concentrations were determined by Bradford assay (Sigma®, B6916) and extracts were analyzed by Western blot.

GST protein purification and GST pulldown

GST fusion proteins were expressed in *Escherichia coli* BL21 (Stratagene®), purified using standard procedures and stored at -80°C. L3MBTL3, L3MBTL3 NTD, L3MBTL3 CTD, NOTCH1 ICD ΔOP, dL(3)mbt and dNICD proteins were *in vitro* translated in the presence of [^{35}S] methionine (Perkin-Elmer®, NEG709A500UC) using the reticulocyte lysate-coupled transcription/translation system (Promega®, L4610) accordingly to manufacturer's instructions. GST fusion proteins were immobilized with Glutathione Sepharose 4 Fast Flow (GE Healthcare®, 17-5132-01) and incubated together with the *in vitro* translated proteins in buffer A (40 mM HEPES at pH 7.5, 5 mM $MgCl_2$, 0.2 mM EDTA, 0.5% NP-40, 100 mM KCl) under rotation for 2 hours at 4°C. Beads were washed three times with buffer A, five times with buffer B (40 mM Hepes pH 7.9, 5 mM $MgCl_2$, 0.2 mM EDTA, 0.5% NP-40, 300 mM KCl) and twice with PBS. Beads were resuspended in Laemmli sample buffer and, after boiling, proteins were resolved by SDS-PAGE. Gels were then dried and exposed to X-ray films.

CRISPR/Cas9-mediated genome editing

CRISPR/Cas9 guide sequences (listed in Table EV2) targeting the *RBPJ* and *L3MBTL3* genes were designed and cloned into the lentiCRISPR CRISPR/Cas9 plasmid (Addgene®, 49535), as previously described (Shalem *et al*, 2014, Wang *et al*, 2014b). The resulting vectors were transfected into U87-MG or MDA-MB-231 cells by lentiviral infection and single cell clones were established upon puromycin selection (2 μg ml^{-1}; Sigma®, P8833). Genome editing was confirmed by PCR and DNA sequencing and gene knockout (KO) was confirmed by Western blotting analysis.

ChIP-seq experiments in MDA-MB-231 cells

The chromatin immuno-precipitation methods are described in the main Materials and Methods section. For ChIP-seq, multiplexed ChIP-seq libraries were prepared at University of Michigan DNA Sequencing Core. 50-cycle single-end sequencing runs were performed on Illumina® HiSeq 2500 at a sequencing depth of 30-40 million aligned reads per sample. Sequenced reads were preprocessed to trim adaptor sequences (Trimmomatic) and then aligned to human reference genome (hg19) using the BWA software (version 0.7.15). Only uniquely mapped reads were used in downstream analyses. Duplicated ChIP-seq samples were processed with Model-based Analysis for ChIP-seq 2 (MACS2) to identify peaks using the default parameters. Peaks were annotated to their nearest gene using GREAT software (McLean *et al*, 2010). Peak overlap was calculated with the criterion that there is at least a 1-bp overlap between tested peaks. Pathway analysis was performed using the GREAT based on a binomial test *P* value < 0.05. Peak tracks were displayed in Integrated Genome Browser (Freese *et al*, 2016). The ChIP-Seq data have been deposited in NCBI's Gene Expression Omnibus (Edgar *et al*, 2002) and are accessible through GEO Series accession number GSE100375: https://www.ncbi.nlm.nih.gov/geo/query/acc.cgi?acc=GSE100375.

Analysis of the *Drosophila* ChIP-seq and ChIP-chip data

ChIP-seq reads were downloaded as SRA-archives from NCBI's Gene Expression Omnibus (GEO) site. After extraction of archives into Fastq files, these were used for alignment against a precompiled dm3 reference index using BOWTIE (Langmead, 2010) downloaded from the BOWTIE homepage (http://bowtie-bio.sourceforge.net/index.shtml). Mapping was done with parameter settings *-m 1* and *-k 1*. Unambiguously mapped and unique reads were kept for subsequent analyses and converted to BAM format using Samtools (Li *et al*, 2009). Peak calling was done with Macs version 1.4 with standard settings against corresponding input samples as control (Zhang *et al*, 2008). All downstream analyses were done in R/BioConductor (http://www.bioconductor.org) (Gentleman *et al*, 2004). We made use of the following R/BioConductor packages: *GenomicRanges* was used for general manipulation of genomic intervals such as identification of overlapping intervals. *GenomicFeatures* was used for handling of transcripts (Lawrence *et al*, 2013) and *Rsamtools* for import of reads into R. After read extension continuous coverage vectors were calculated and exported into bigwig and bed files using *rtracklayer* for visualization in genome browsers (Lawrence *et al*, 2009). Browser snap shots were generated with the *Gviz* BioConductor package. In the analysis of peak overlaps, we treated two peak intervals as being overlapping in case their overlap was 1 bp or more.

ChIP-chip data files were downloaded as Nimblegen PAIR files and were analyzed with the Python version of MA2C (Song *et al*, 2007) with the following settings: normalization: simple; peak detection: pvalue; threshold: 0.001; min. probes: 5; bandwidth: 500 bp; max. distance: 250 bp. The continuous MA2C-score was exported as bigwig and used for visual representation in genome browsers and detected peaks were imported into R for downstream analysis. The data sets used in our analysis are: dL(3)mbt ChIP-seq in Kc167 cells [GSE62904) (Li *et al*, 2015)] and Su(H) ChIP-chip in 3rd instar larval discs [GSE68614 (Zacharioudaki *et al*, 2016)].

Statistical analysis of the overlaps observed for the binding sites and the bound genes in the ChIP experiments

To analyze the significance of the overlaps observed between the dL(3)mbt/L3MBTL3 and Su(H)/RBPJ binding sites, we make the assumption that there are 50000 possible binding sites in the genome (a conservative assumption) and we assess the extent to which the observed overlaps are larger than expected at random using a two-sided Fisher Exact test. We note that as one assumes a higher number of possible binding sites, the significance of observing a larger than expected overlap becomes greater. For the analysis of the bound gene overlaps, we assess the extent to which the observed overlaps are larger than expected at random using a two-sided Fisher Exact test assuming that there are 20000 and 17000 genes in the human and *Drosophila* genomes, respectively.

Appendix Supplementary Figure Legends

Appendix Figure S1. L3MBTL3 interacts with RBPJ.

A L3MBTL3 interacts with RBPJ. IP of HA-tagged RBPJ (top panels) or SBP-FLAG-tagged L3MBTL3 (bottom panels) in HEK293T cells. MYC-L3MBTL3 co-purifies with HA-RBPJ (top panels) and HA-RBPJ co-purifies with SBP-FLAG-L3MBTL3 (bottom panels). The experiment was independently replicated twice.

B Schematic representation of the L3MBTL3 proteins used in panels C and D. The L3MBTL3 protein (XP_006715641.1) consists of: a C2C2 zinc finger (ZnF #1; CDD: 128717), three MBT domains (CDD: 214723), a C2H2 zinc finger (ZnF #2; CDD: 201844) and a sterile α motif domain (SAM; CDD: 197735).

C GST pulldown showing that L3MBTL3 directly interacts with RBPJ. *In vitro* transcribed and translated L3MBTL3 or NOTCH1 ICD ΔOP was incubated with bacterially purified GST-RBPJ or GST alone pre-bound to glutathione beads. Proteins were resolved via SDS-

PAGE and signals acquired via X-ray exposure. NOTCH1 ICD ΔOP was used as positive control. The experiment was independently replicated twice.

D The NTD domain of L3MBTL3 strongly interacts with RBPJ. *In vitro* transcribed and translated L3MBTL3 NTD, CTD or NOTCH1 ICD ΔOP were incubated with bacterially purified GST-RBPJ or GST alone pre-bound to glutathione beads. Proteins were resolved via SDS-PAGE and signals acquired via X-ray exposure. The NOTCH1 ICD ΔOP was used as positive control. The experiment was independently replicated twice.

WB: Western blot; IP: immuno-precipitation; EV: Empty Vector control.

Appendix Figure S2. Notch signaling tone is low in U87-MG cells.

A Treatment with γ-secretase inhibitor (GSI) has no effect on the expression of Notch target genes in U87-MG cells. Expression analysis of Notch target genes in *L3MBTL3* WT (Control) or *L3MBTL3* knockout (KO) (sg-*L3MBTL3*) U87-MG cells upon GSI treatment. Shown are means ±s.d. of duplicate experiments after experiment effects were removed. *NS*: Not Significant; two-way *ANOVA* model on log-transformed data.

B Overexpression of a dominant negative mutant of MAML (DN-MAML) does not influence the expression of Notch target genes in U87-MG cells. Expression analysis of Notch target genes in U87-MG cells upon overexpression of DN-MAML. Control: empty vector. Shown are means ±s.d. of triplicate experiments. *NS*: Not Significant; two-sample *T*-test on log-transformed data.

C Notch target genes are induced by NOTCH1 ICD in U87-MG cells. Expression analysis of Notch target genes in U87-MG cells upon overexpression of either NOTCH1 ICD or EGFP control (Control). Shown are means ±s.d. of triplicate experiments. [*] $P < 0.05$, [**] $P < 0.01$; two-sample *T*-test on log-transformed data.

Appendix Figure S3. L3MBTL3 and RBPJ co-localize at the Notch-responsive elements of Notch target genes in U87-MG cells.

A Representation of RBPJ-binding sites previously identified in CUTLL1 cells (Wang *et al*, 2014a) (turquoise bars) and of the genomic regions (magenta bars) analyzed in our ChIP studies. Distances in base pairs (bp) relative to the transcriptional start site (TSS) are indicated. Primer sequences are shown in Table EV2.

B RBPJ and L3MBTL3 co-localize at two distal *HES1* enhancers. ChIP analyses of endogenous RBPJ and L3MBTL3 in U87-MG cells were performed for two previously described distal RBPJ-bound enhancers of *HES1* (Wang *et al*, 2014a). Shown are means ±s.d. of triplicate experiments.

C L3MBTL3 localizes at the proximal and distal Notch-responsive elements of Notch target genes in U87-MG cells. ChIP analysis of L3MBTL3 in U87-MG cells transfected with plasmid encoding a TET-ON-dependent, doxycycline (DOX)-inducible HA-tagged L3MBTL3 protein. ChIP was performed using an HA antibody. Shown are means ±s.d. of duplicate or triplicate experiments.

D L3MBTL3 depletion does not influence RBPJ occupancy in U87-MG cells. ChIP analyses of RBPJ and L3MBTL3 in *L3MBTL3* KO U87-MG cells. Shown are means ±s.d. of duplicate experiments. Our results indicate that the L3MBTL3 antibody is specific.

E Western blot analysis validates the overexpression of L3MBTL3 and the shRNA-mediated depletion of RBPJ.

F Expression analysis of *OCT4*, which is not a Notch target gene, in U87-MG cells upon *RBPJ* knockdown and/or overexpression of L3MBTL3. Shown are means ±s.d. of triplicate experiments. *P* values were estimated via an *ANOVA* model on log-transformed data; *NS*: Not Significant.

Panels B, C and D: distance in base pairs (bp) relative to the transcriptional start site (TSS) is indicated below the gene names; Chrom8 was used as negative control (NEG).

Appendix Figure S4. The RBPJ/L3MBTL3 interaction is required for repression of Notch target genes in MDA-MB-231 cells.

A GSI treatment does not influence the expression of Notch target genes in MDA-MB-231 cells. Shown are means ±s.d. of duplicate experiments. *NS*: Not Significant; two-sample *T*-test on log-transformed data.

B Notch target genes are induced by NOTCH1 ICD in MDA-MB-231 cells. Control: EGFP. Shown are means ±s.d. of triplicate experiments. [**] $P < 0.01$; two-sample *T*-test on log-transformed data.

C *RBPJ* or *L3MBTL3* knockdown leads to de-repression of Notch target genes in MDA-MB-231 cells. Expression analysis of Notch target genes upon *RBPJ* or *L3MBTL3* knockdown. Shown are means ±s.d. of triplicate experiments. [*] $P < 0.05$, [**] $P < 0.01$; one-way *ANOVA* model on log-transformed data.

D L3MBTL3 binds two distal enhancers of *HES1* in MDA-MB-231 cells. ChIP analyses were performed in MDA-MB-231 cells at two previously described distal RBPJ-bound enhancers of *HES1* (Wang *et al*, 2014a). Shown are means ±s.d. of triplicate experiments.

E L3MBTL3 binds the proximal Notch-responsive elements of *HES1* and *HEY2* in a RBPJ-dependent manner in MDA-MB-231 cells. ChIP analyses of RBPJ or L3MBTL3 upon *RBPJ* knockdown. Shown are means ±s.d. of one experiment measured twice.

F Repression of Notch target genes by L3MBTL3 is RBPJ-dependent. Expression analysis of *HES1* and *HEY2* upon overexpression of L3MBTL3 in RBPJ depleted MDA-MB-231 cells. Shown are means ±s.d. of quadruplicate experiments. *P* values were estimated via a one-way *ANOVA* model on log-transformed data where the difference of differences was tested, which is equivalent to testing the interaction in a two-way *ANOVA* model. Inset: Western blot analysis validates the overexpression of L3MBTL3 and the shRNA-mediated depletion of RBPJ.

G L3MBTL3 occupancy at the proximal Notch-responsive elements of Notch target genes depends on the L3MBTL3-(1-64) domain. MDA-MB-231 cells were transfected with V5-L3MBTL3 WT, V5-L3MBTL3-Δ(1-64) or with empty vector (Control) and ChIP experiments were performed using RBPJ, L3MBTL3 or V5 antibody. Shown are means ±s.d. of duplicate experiments. We note that the L3MBTL3 antibody immuno-precipitates both endogenous and V5-tagged L3MBTL3.

H The L3MBTL3/RBPJ interaction is required for the repression of Notch target genes by L3MBTL3 in MDA-MB-231 cells. Cells were transfected with L3MBTL3 WT, L3MBTL3-Δ(1-64) or LacZ control (Control) and expression of Notch target genes was analyzed via qPCR. Shown are means ±s.d. of duplicate experiments measured twice each. *P* values were estimated via a one-way *ANOVA* model on log-transformed data.

Panels D, E and G: distance in base pairs (bp) relative to the transcriptional start site (TSS) is indicated below the gene names; Chrom8 was used as negative control (NEG).

Appendix Figure S5. L3MBTL3 represses Notch target genes in mature T-cells.

A Cleaved NOTCH1 is not detectable in mouse hybridoma mature T-cells. Whole cell extracts from both Beko, a mouse pre–T cell line that is characterized by constitutively active Notch signaling (Liefke *et al*, 2010) and mouse hybridoma mature T-cells (MT) were analyzed by Western blot using an antibody that only recognizes the cleaved NOTCH1 ICD (NICD1). GAPDH was used as a loading control. The experiment was independently replicated twice.

B *Hes1* and *Hey1* Notch target genes are induced by Bio-tagged NOTCH1 ICD ΔOP in mature T-cells. Control: Bio empty vector control. Shown are means ±s.d. of quadruplicate experiments after experiment effects were removed. [**] $P < 0.01$; paired *T*-test on log-transformed data.

C Western blot showing the expression of Bio-tagged NOTCH1 ICD ΔOP. RNAPII was used as loading control.

D Expression analysis of Notch target genes upon *L3mbtl3* knockdown in a mouse hybridoma mature T-cell line. *Hey1* and *Hes1* Notch target genes are de-repressed upon *L3mbtl3* knockdown in mouse hybridoma mature T-cells. Shown are means ±s.d. of duplicate experiments measured twice each. Statistical significances of the difference between sh-Scr and sh-*L3mbtl3* #1 or #2 were estimated via a two-way *ANOVA* model on log-transformed data.

E Western blot showing the downregulation of L3MBTL3 in mouse hybridoma mature T-cells upon knockdown of *L3MBTL3*. RNAPII was used as loading control.

F Expression analysis of Notch target genes upon *L3mbtl3* knockdown in Beko cells. *Hey1* and *Hes1* Notch target genes are not de-repressed upon *L3mbtl3* knockdown in this mouse pre-T cell line that is characterized by constitutively active Notch signaling (Liefke *et al*, 2010). Shown are means ±s.d. of quadruplicate experiments after experiment effects were removed. [**] $P < 0.01$, *NS*: Not Significant; two-way *ANOVA* model on log-transformed data.

Appendix Figure S6. L3MBTL3 negatively regulates H3K4me2 at the *HES1* locus.

A ChIP analysis of H3K4me2 at the enhancer of *HES1* in RBPJ-depleted U87-MG cells. Shown are means ±s.d. of triplicate experiments.

B ChIP analysis of H3K4me2 at the *HES1* locus upon overexpression of L3MBTL3 WT in *L3MBTL3* KO U87-MG cells. Shown are means ±s.d. of duplicate experiments. Control: empty vector.

Appendix Figure S7. *Drosophila* dL(3)mbt and Su(H) co-localize at Notch target genes.

Snapshots showing the genomic co-localization of dL(3)mbt and Su(H) at the *E(spl)* (panel A) and the *lola* (panel B) loci.

Appendix Figure S8. Loss-of-*dL(3)mbt* leads to upregulation of *E(spl)mγ*.

Analysis of the expression of *E(spl)mγ-HLH-GFP* in the optic lobes of WT and *dL(3)mbt* mutant third instar larvae. $dL(3)mbt^{GM76}$ mutant is in heterozygosity with *Df(3R)D605*, a *dL(3)mbt* deficiency line in which the whole *dL(3)mbt* locus is deleted. WT and mutant larvae were cultured at 31°C, which is non-permissive for the temperature-sensitive hypomorphic $dL(3)mbt^{GM76}$ mutant. Larval brains were dissected 72 hours after larval hatching and processed for *Discs large* (*Dlg*) and *Deadpan* (*Dpn*) immuno-stainings. We used *Dlg* as a cortical marker, *Dpn* as a marker of central brain and optic lobe neuroblasts, and *E(spl)mγ-HLH-GFP as a* Notch-reporter. The images were selected based on the distance from the most dorsal region and they represent comparable brain depths. Representative images of confocal cross sections of both the apical (A-H) and medial (I-P) regions are shown. In the optic lobe of WT larvae, high level of *E(spl)mγ-HLH-GFP* activity is mainly detected in neuroepithelial cells located either in the inner proliferation centers (yellow arrows in C-D) or at the tips of outer proliferation centers (yellow arrows in K-L) where neuroepitelial cells differentiate into neuroblasts. In the optic lobe of *dL(3)mbt* mutant larvae, the previously described massive expansion of the neuroepithelia (Richter *et al*, 2011) is accompanied by a strong increase in the number of *E(spl)mγ-HLH-GFP* positive cells in different regions of the distorted, tumorigenic larval brain (yellow arrows in G-H and O-P). At least 10 brains for each genotype were analyzed. Scale bars: 20μm.

Appendix Figure S9. Synergy between gain-of-*Notch* and loss-of-*dL(3)mbt* in the *Drosophila* eye imaginal disc.

A-L Animals were grown at 31°C, which is non-permissive for the temperature-sensitive hypomorphic *dL(3)mbt*^{GM76} mutant. Eye imaginal discs dissected from third instar larvae were stained with α-dNICD (green) and α-elav (red; to mark differentiated cells) antibodies. *E1-Gal4* is an eye-specific *UAS* driver.

D-F Heterozygous *dL(3)mbt*^{GM76} mutant has no detectable effect on the eye imaginal disc and is comparable to *E1-Gal4* control.

G-I Ectopic expression of dNICD results in enlarged and distorted eye discs.

J-L Heterozygous *dL(3)mbt*^{GM76} and dNICD overexpression synergize to cause massively overgrown, distorted and largely undifferentiated (elav-negative) eye discs.

At least 10 discs for each genotype were analyzed. Representative images are shown. Scale bars: 100μm.

Appendix Figure S10. Reduction of *cut* expression domain by dL(3)mbt in the wing disc is not a consequence of apoptosis.

Wing discs expressing *UAS-p35* (a-c) or *UAS-p35;UAS-HA-dL(3)mbt* (d-f) under the *vg-Gal4* driver at 25°C were stained for cut (red) and HA (blue). The baculovirus P35 protein functions as a caspase inhibitor, which prevents apoptotic death (Hay *et al*, 1994). Wing discs expressing HA-dL(3)mbt along with anti-apoptotic P35 show the same reduction of cut staining seen in *vg-Gal4;UAS-dL(3)mbt;UAS-GFP* discs (Fig 6D), indicating that apoptosis does not contribute to the inhibition of the Notch target gene *cut*. Control animals expressing *UAS-p35* alone appear wild-type. Insets below each panel show a closer view of the D-V boundary. At least 10 discs for each genotype were analyzed. Representative images are shown. Scale bars: 100μm.

Appendix Figure S11. dL(3)mbt overexpression in the dorso-ventral (D-V) boundary of the wing imaginal disc results in the inhibition of *cut* induced by ectopic dNICD.

Wing discs expressing *UAS-dNICD;UAS-GFP;UAS-GFP* (A-D) *or UAS-dNICD;UAS-HA-dL(3)mbt;UAS-GFP* (E-H) under the *vg-Gal4* driver at 25°C were stained for cut (red) and HA (blue). GFP marks the *vg-Gal4* expression domain. Note that *UAS-dNICD;UAS-GFP;UAS-GFP* contains two copies of *UAS-GFP* to account for potential effects associated with *UAS* titration. At least 30 discs for each genotype were analyzed. Representative images are shown. Scale bars: 100μm.

Appendix Figure S12. dL(3)mbt reduces cut expression in the anterior-posterior (A-P) boundary of the wing disc in a cell-autonomous manner.

UAS-HA-dL(3)mbt (panels D-F and J-L)*, UAS-GFP* (panels D-F) and/or *UAS-dNICD* (panels G-L) were expressed in a *ptc-Gal4;tub-Gal80^{ts}* background. The *ptc-Gal4;tub-Gal80^{ts}* control is shown in panels A-C. Larvae were reared at 18°C (permissive temperature for *Gal80^{ts}*) and transferred to 31°C (restrictive temperature for *Gal80^{ts}*) 26 hours prior to harvesting for staining for cut (red; panels A, D, G and J) and HA (blue; panels B, E, H and K). Merged images are shown in panels C, F, I and L. Insets below each panel show a closer view of the D-V boundary region with yellow arrows in D-F pointing to the region of cut suppression at the intersection of the A-P and D-V boundaries. At least 10 discs for each genotype were analyzed. Representative images are shown. Scale bars: 100μm.

Appendix Supplementary References

Collins KJ, Yuan Z, Kovall RA (2014) Structure and function of the CSL-KyoT2 corepressor complex: a negative regulator of Notch signaling. *Structure* 22: 70-81

Edgar R, Domrachev M, Lash AE (2002) Gene Expression Omnibus: NCBI gene expression and hybridization array data repository. *Nucleic Acids Res* 30: 207-10

Fehon RG, Kooh PJ, Rebay I, Regan CL, Xu T, Muskavitch MA, Artavanis-Tsakonas S (1990) Molecular interactions between the protein products of the neurogenic loci Notch and Delta, two EGF-homologous genes in Drosophila. *Cell* 61: 523-34

Freese NH, Norris DC, Loraine AE (2016) Integrated genome browser: visual analytics platform for genomics. *Bioinformatics* 32: 2089-95

Gentleman RC, Carey VJ, Bates DM, Bolstad B, Dettling M, Dudoit S, Ellis B, Gautier L, Ge Y, Gentry J, Hornik K, Hothorn T, Huber W, Iacus S, Irizarry R, Leisch F, Li C, Maechler M, Rossini AJ, Sawitzki G et al. (2004) Bioconductor: open software development for computational biology and bioinformatics. *Genome Biol* 5: R80

Hay BA, Wolff T, Rubin GM (1994) Expression of baculovirus P35 prevents cell death in Drosophila. *Development* 120: 2121-9

Jung C, Mittler G, Oswald F, Borggrefe T (2013) RNA helicase Ddx5 and the noncoding RNA SRA act as coactivators in the Notch signaling pathway. *Biochim Biophys Acta* 1833: 1180-9

Langmead B (2010) Aligning short sequencing reads with Bowtie. *Curr Protoc Bioinformatics* Chapter 11: Unit 11 7

Lawrence M, Gentleman R, Carey V (2009) rtracklayer: an R package for interfacing with genome browsers. *Bioinformatics* 25: 1841-2

Lawrence M, Huber W, Pages H, Aboyoun P, Carlson M, Gentleman R, Morgan MT, Carey VJ (2013) Software for computing and annotating genomic ranges. *PLoS Comput Biol* 9: e1003118

Li H, Handsaker B, Wysoker A, Fennell T, Ruan J, Homer N, Marth G, Abecasis G, Durbin R, Genome Project Data Processing S (2009) The Sequence Alignment/Map format and SAMtools. *Bioinformatics* 25: 2078-9

Li L, Lyu X, Hou C, Takenaka N, Nguyen HQ, Ong CT, Cubenas-Potts C, Hu M, Lei EP, Bosco G, Qin ZS, Corces VG (2015) Widespread rearrangement of 3D chromatin organization underlies polycomb-mediated stress-induced silencing. *Mol Cell* 58: 216-31

Liefke R, Oswald F, Alvarado C, Ferres-Marco D, Mittler G, Rodriguez P, Dominguez M, Borggrefe T (2010) Histone demethylase KDM5A is an integral part of the core Notch-RBP-J repressor complex. *Genes Dev* 24: 590-601

Longo PA, Kavran JM, Kim MS, Leahy DJ (2013) Transient mammalian cell transfection with polyethylenimine (PEI). *Methods Enzymol* 529: 227-40

Maillard I, Weng AP, Carpenter AC, Rodriguez CG, Sai H, Xu L, Allman D, Aster JC, Pear WS (2004) Mastermind critically regulates Notch-mediated lymphoid cell fate decisions. *Blood* 104: 1696-702

McLean CY, Bristor D, Hiller M, Clarke SL, Schaar BT, Lowe CB, Wenger AM, Bejerano G (2010) GREAT improves functional interpretation of cis-regulatory regions. *Nat Biotechnol* 28: 495-501

Oswald F, Rodriguez P, Giaimo BD, Antonello ZA, Mira L, Mittler G, Thiel VN, Collins KJ, Tabaja N, Cizelsky W, Rothe M, Kuhl SJ, Kuhl M, Ferrante F, Hein K, Kovall RA, Dominguez M, Borggrefe T (2016) A phospho-dependent mechanism involving NCoR and KMT2D controls a permissive chromatin state at Notch target genes. *Nucleic Acids Res*

Oswald F, Tauber B, Dobner T, Bourteele S, Kostezka U, Adler G, Liptay S, Schmid RM (2001) p300 acts as a transcriptional coactivator for mammalian Notch-1. *Mol Cell Biol* 21: 7761-74

Richter C, Oktaba K, Steinmann J, Muller J, Knoblich JA (2011) The tumour suppressor L(3)mbt inhibits neuroepithelial proliferation and acts on insulator elements. *Nat Cell Biol* 13: 1029-39

Rual JF, Hirozane-Kishikawa T, Hao T, Bertin N, Li S, Dricot A, Li N, Rosenberg J, Lamesch P, Vidalain PO, Clingingsmith TR, Hartley JL, Esposito D, Cheo D, Moore T, Simmons B, Sequerra R, Bosak S, Doucette-Stamm L, Le Peuch C et al. (2004) Human ORFeome version 1.1: a platform for reverse proteomics. *Genome Res* 14: 2128-35

Shalem O, Sanjana NE, Hartenian E, Shi X, Scott DA, Mikkelsen TS, Heckl D, Ebert BL, Root DE, Doench JG, Zhang F (2014) Genome-scale CRISPR-Cas9 knockout screening in human cells. *Science* 343: 84-7

Song JS, Johnson WE, Zhu X, Zhang X, Li W, Manrai AK, Liu JS, Chen R, Liu XS (2007) Model-based analysis of two-color arrays (MA2C). *Genome Biol* 8: R178

Wang H, Zang C, Taing L, Arnett KL, Wong YJ, Pear WS, Blacklow SC, Liu XS, Aster JC (2014a) NOTCH1-RBPJ complexes drive target gene expression through dynamic interactions with superenhancers. *Proc Natl Acad Sci U S A* 111: 705-10

Wang T, Wei JJ, Sabatini DM, Lander ES (2014b) Genetic screens in human cells using the CRISPR-Cas9 system. *Science* 343: 80-4

Weng M, Golden KL, Lee CY (2010) dFezf/Earmuff maintains the restricted developmental potential of intermediate neural progenitors in Drosophila. *Dev Cell* 18: 126-35

Yang X, Boehm JS, Salehi-Ashtiani K, Hao T, Shen Y, Lubonja R, Thomas SR, Alkan O, Bhimdi T, Green TM, Johannessen CM, Silver SJ, Nguyen C, Murray RR, Hieronymus H, Balcha D, Fan C, Lin C, Ghamsari L, Vidal M et al. (2011) A public genome-scale lentiviral expression library of human ORFs. *Nat Methods* 8: 659-61

Yuan Z, Friedmann DR, VanderWielen BD, Collins KJ, Kovall RA (2012) Characterization of CSL (CBF-1, Su(H), Lag-1) mutants reveals differences in signaling mediated by Notch1 and Notch2. *J Biol Chem* 287: 34904-16

Zacharioudaki E, Housden BE, Garinis G, Stojnic R, Delidakis C, Bray SJ (2016) Genes implicated in stem cell identity and temporal programme are directly targeted by Notch in neuroblast tumours. *Development* 143: 219-31

Zhang Y, Liu T, Meyer CA, Eeckhoute J, Johnson DS, Bernstein BE, Nusbaum C, Myers RM, Brown M, Li W, Liu XS (2008) Model-based analysis of ChIP-Seq (MACS). *Genome biology* 9: R137

Appendix Figure S1. (Rual)

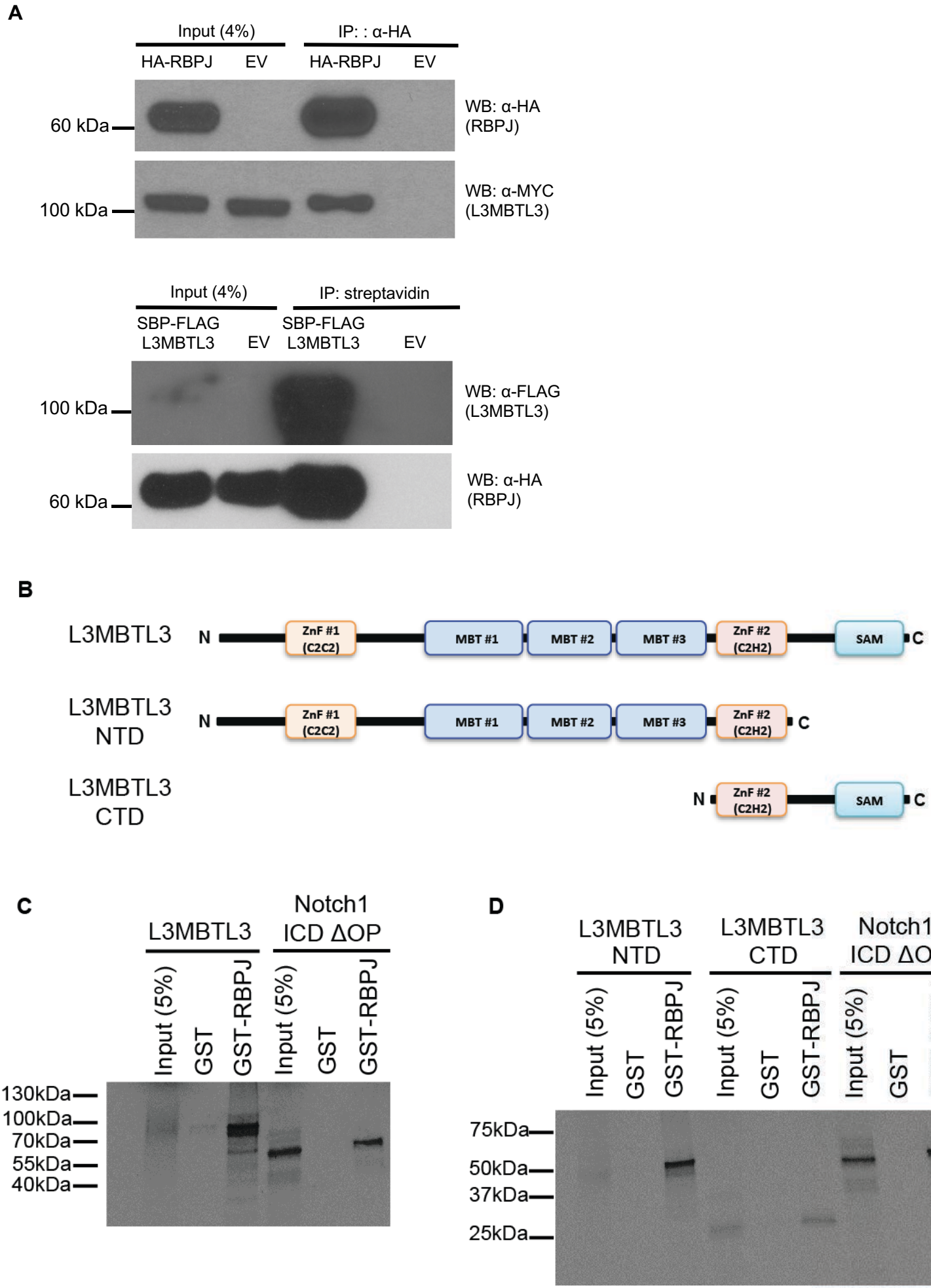

Appendix Figure S2. (Rual)

A

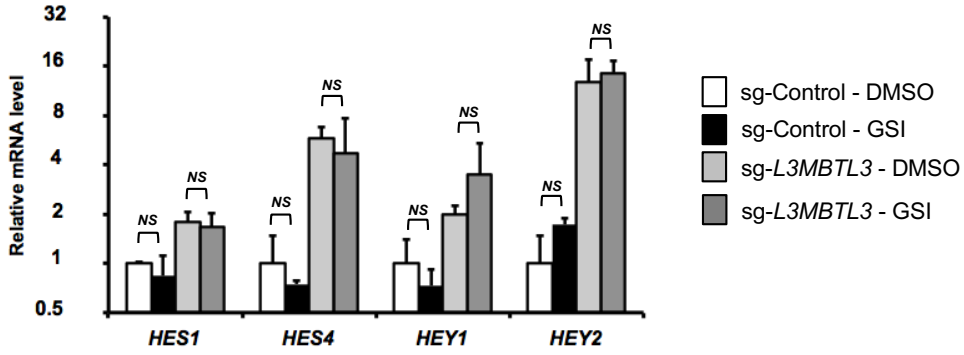

B

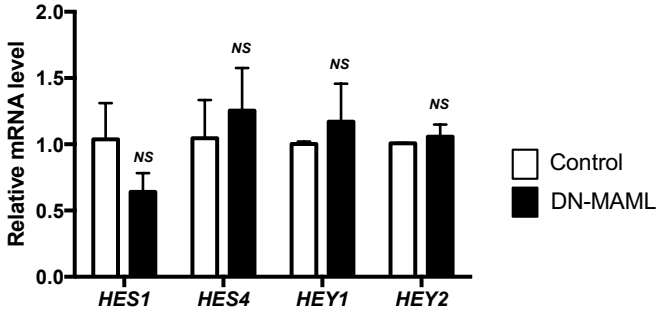

C

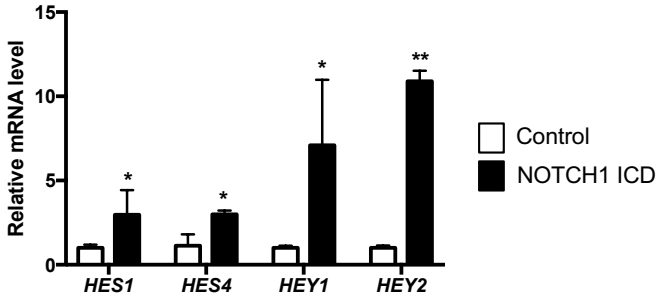

Appendix Figure S3. (Rual)

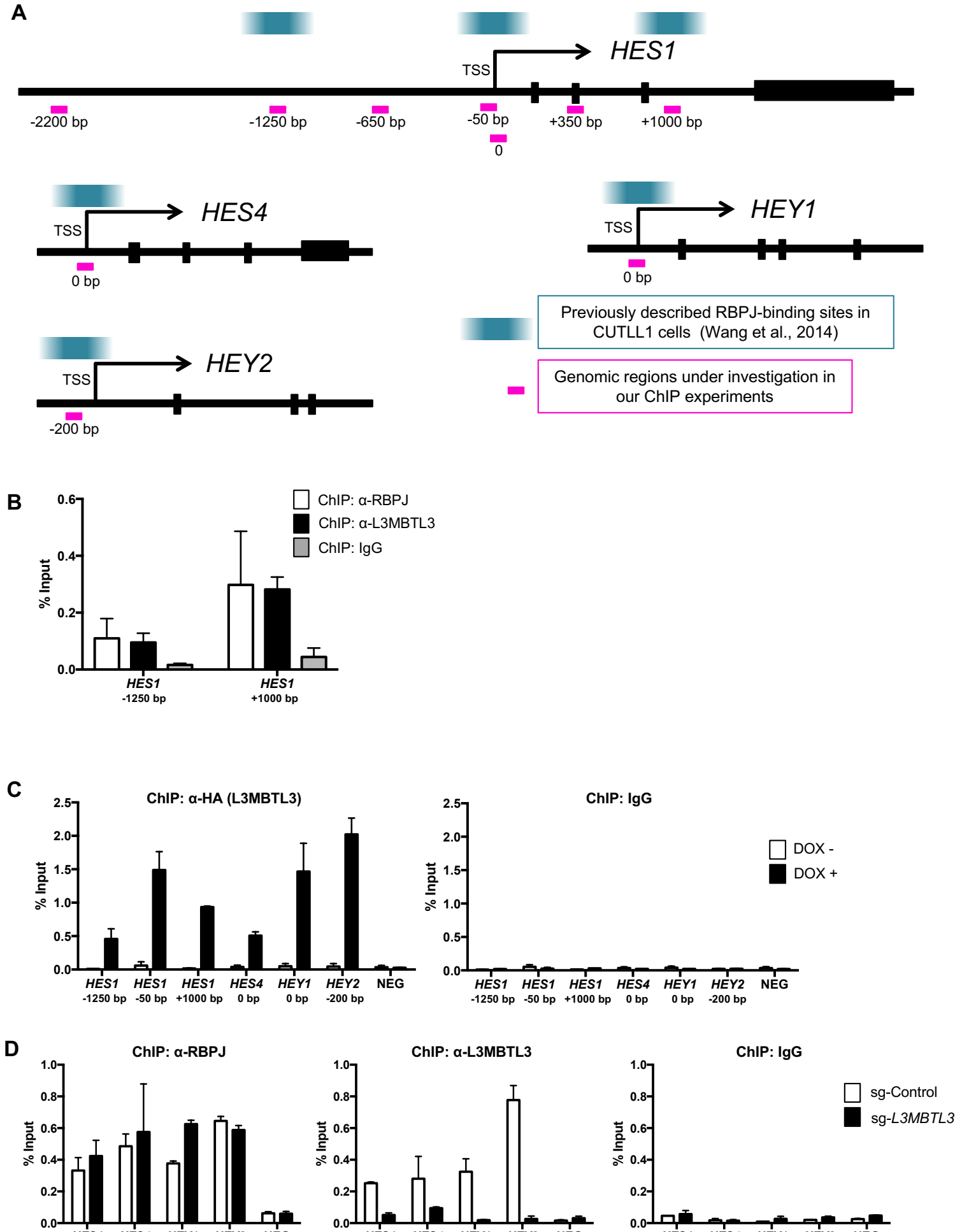

Appendix Figure S3 (continued). (Rual)

E

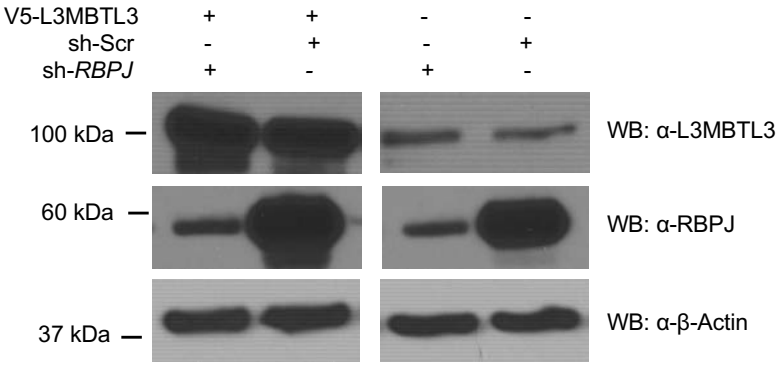

F

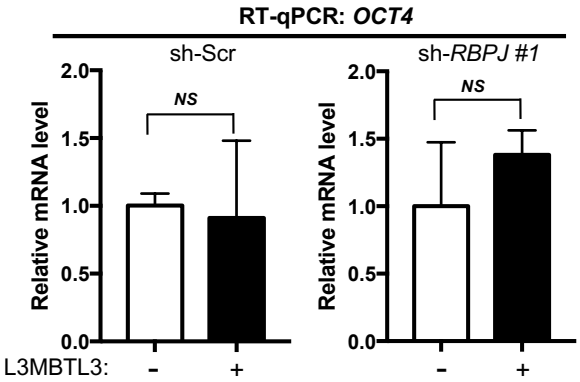

Appendix Figure S4. (Rual)

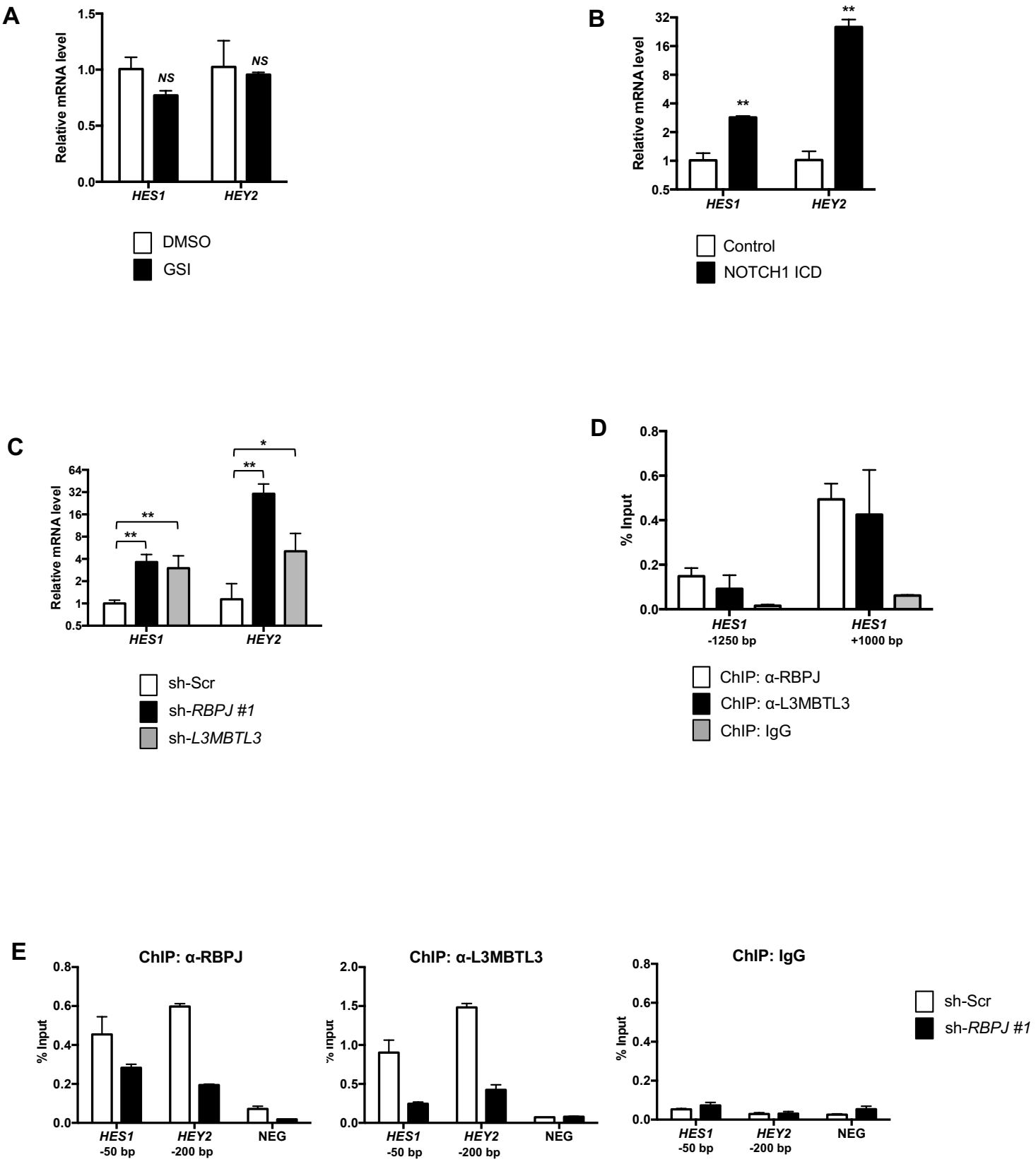

Appendix Figure S4 (continued). (Rual)

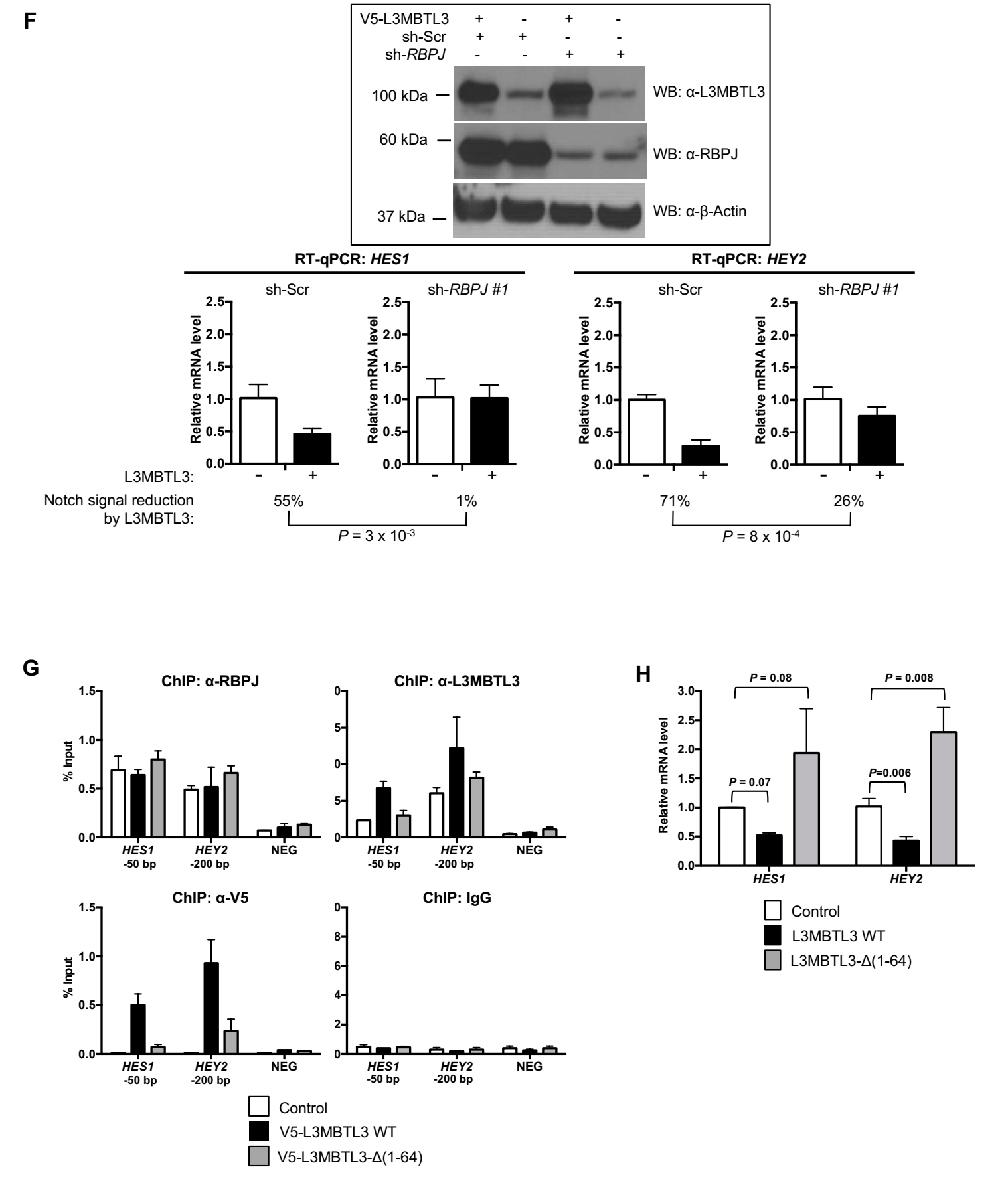

Appendix Figure S5. (Rual)

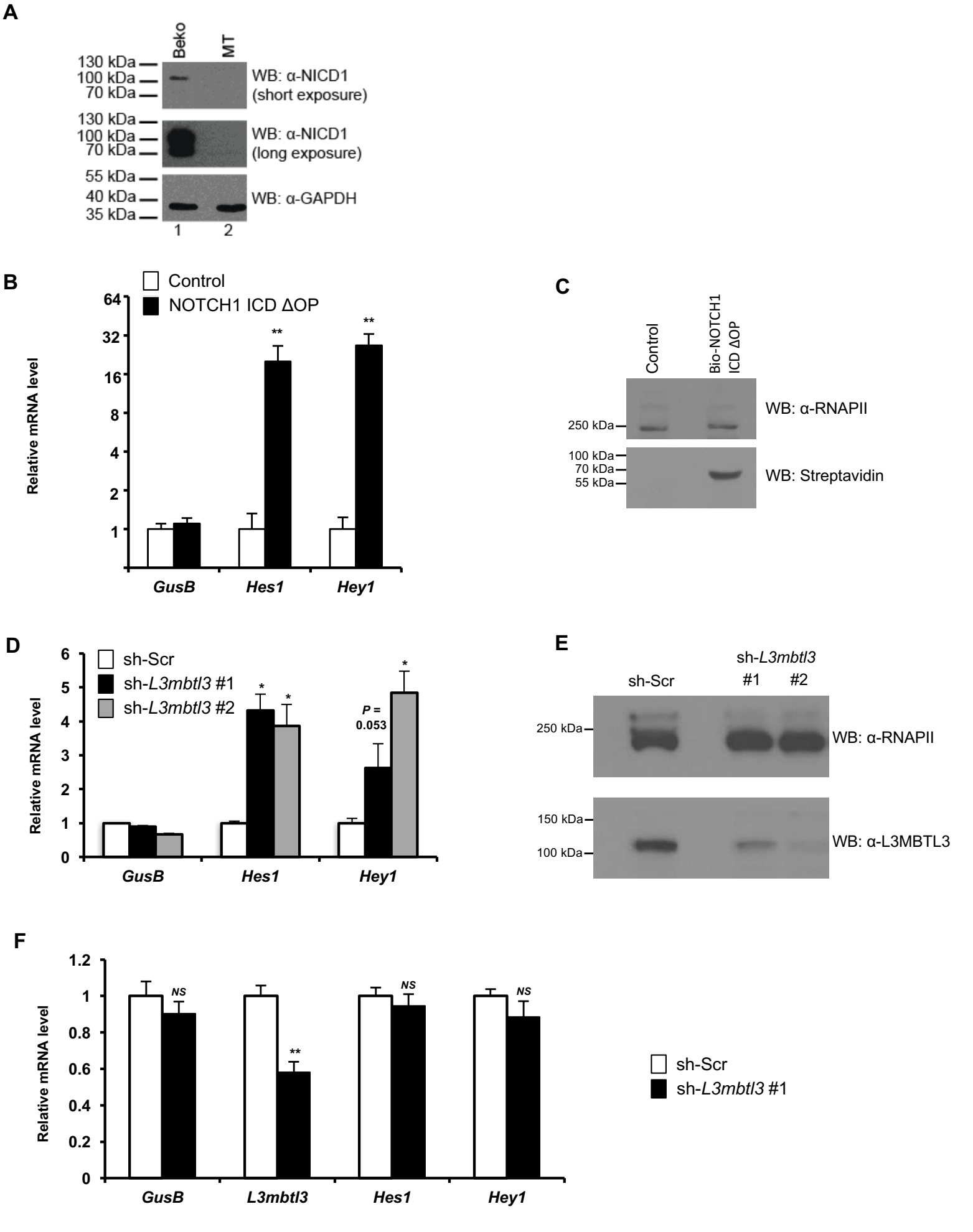

Appendix Figure S6. (Rual)

A

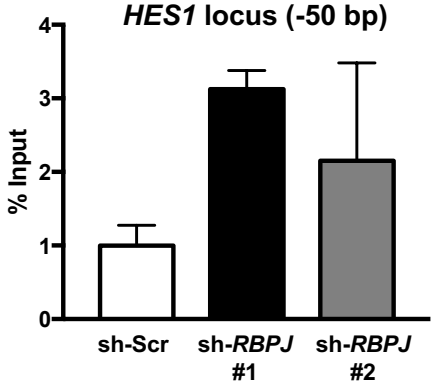

B

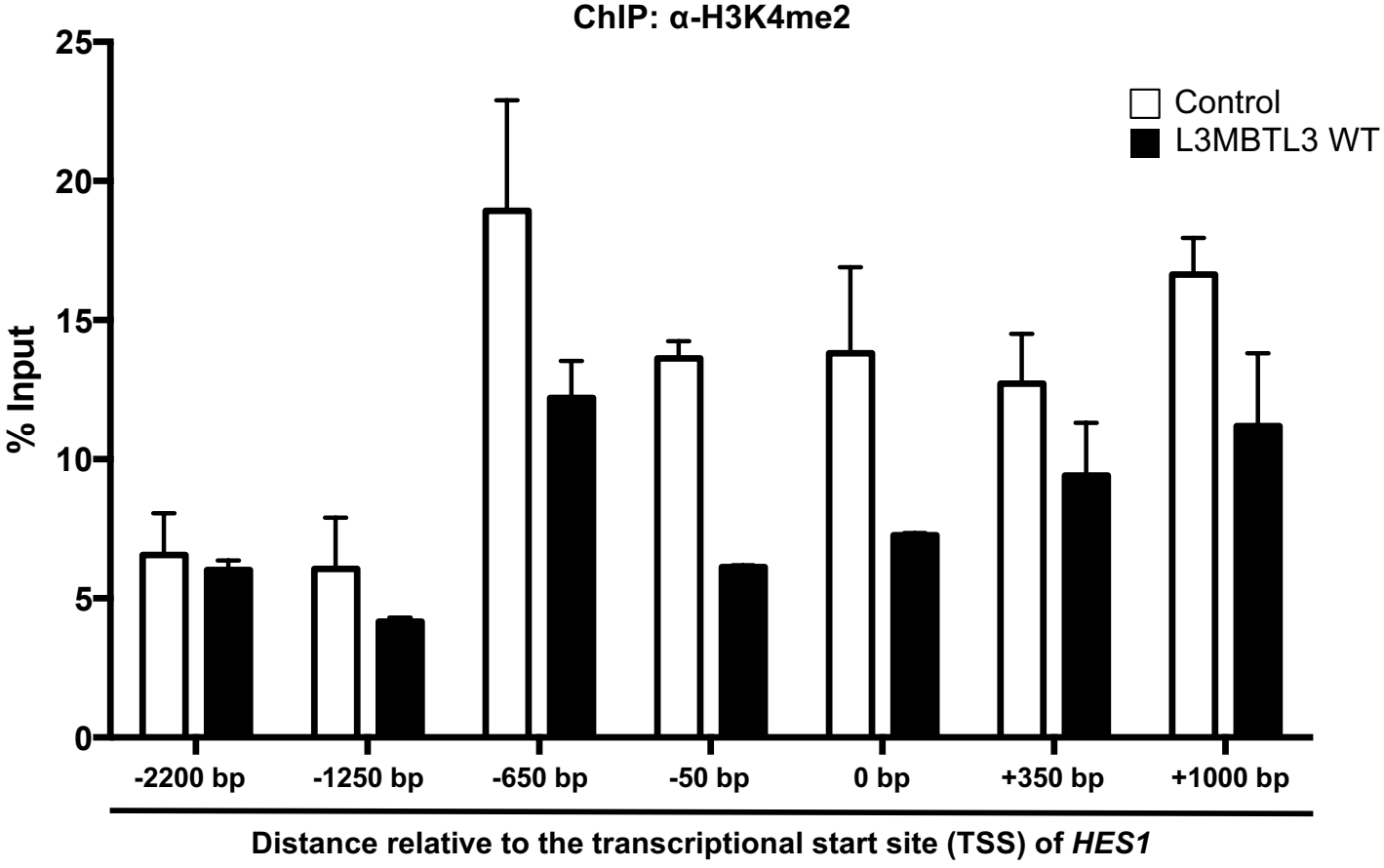

Appendix Figure S7. (Rual)

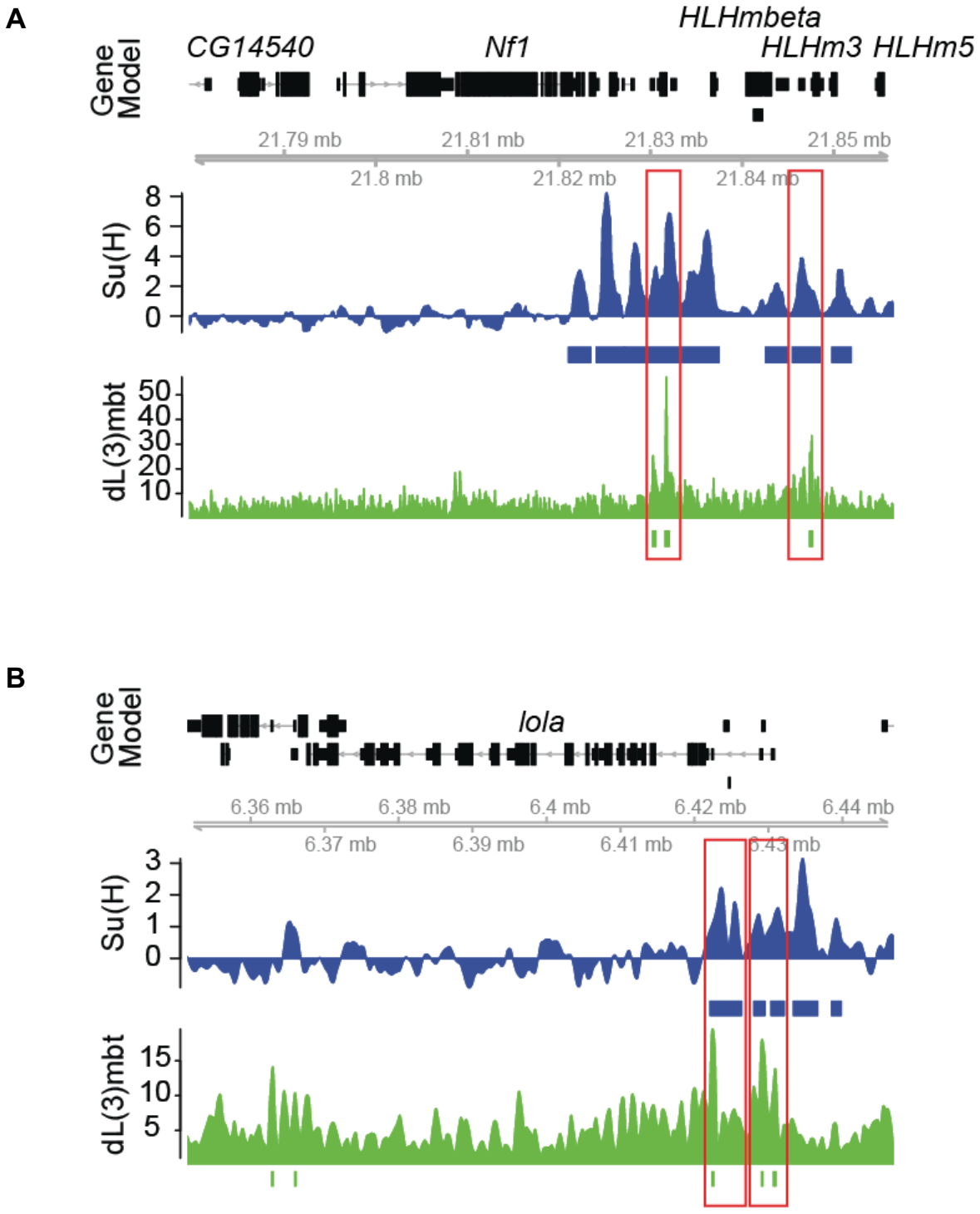

Appendix Figure S8. (Rual)

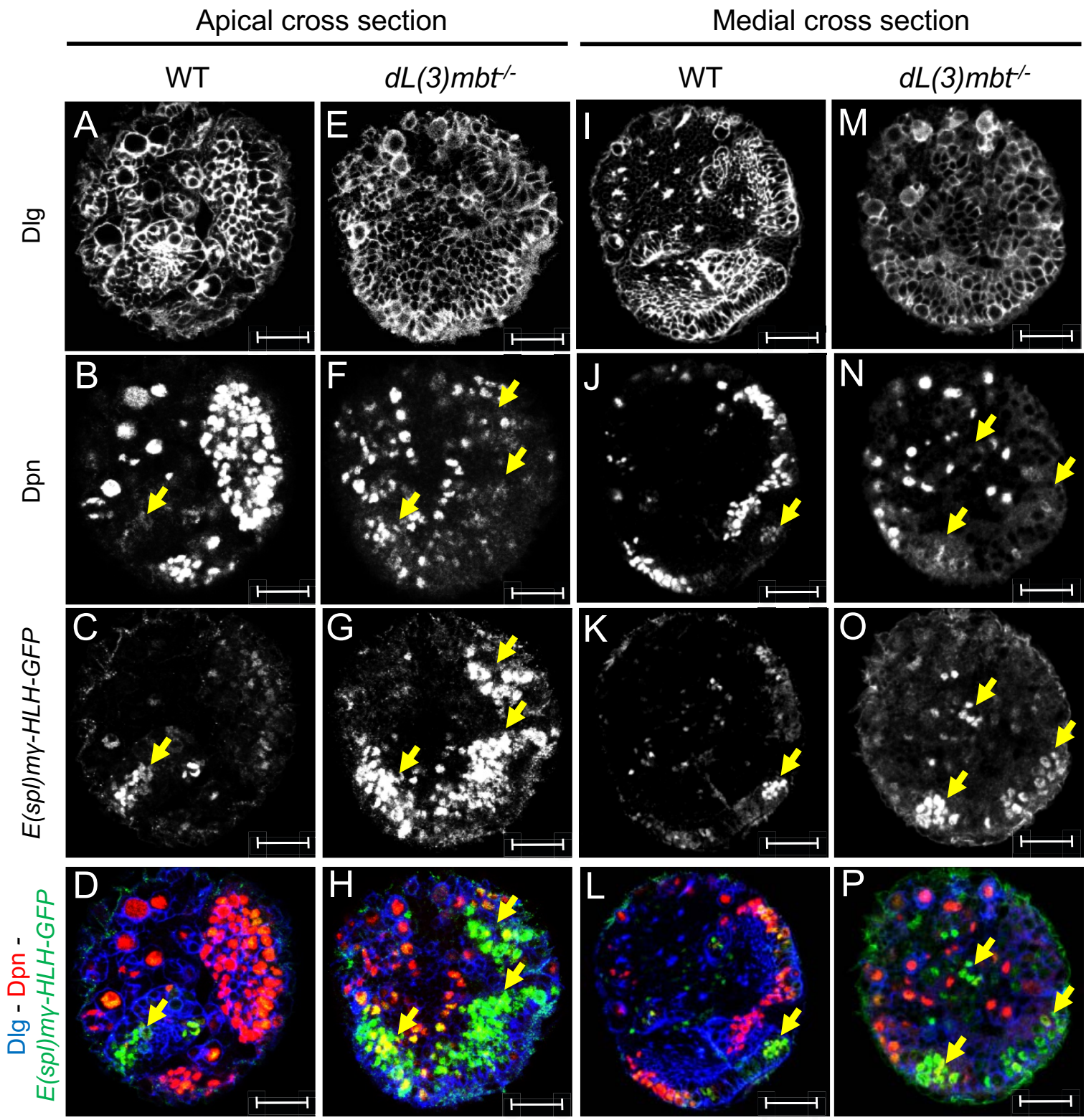

Appendix Figure S9. (Rual)

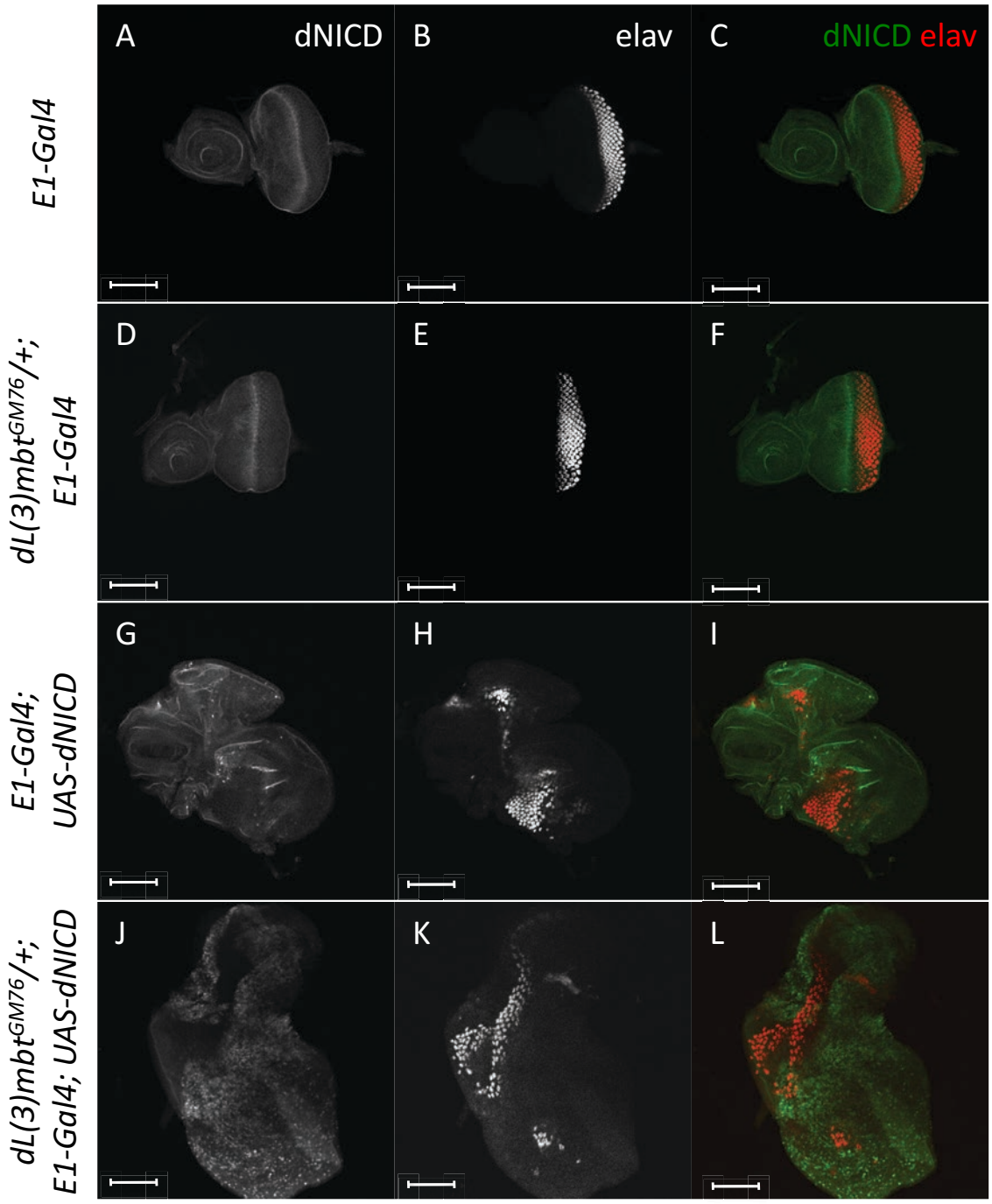

Appendix Figure S10. (Rual)

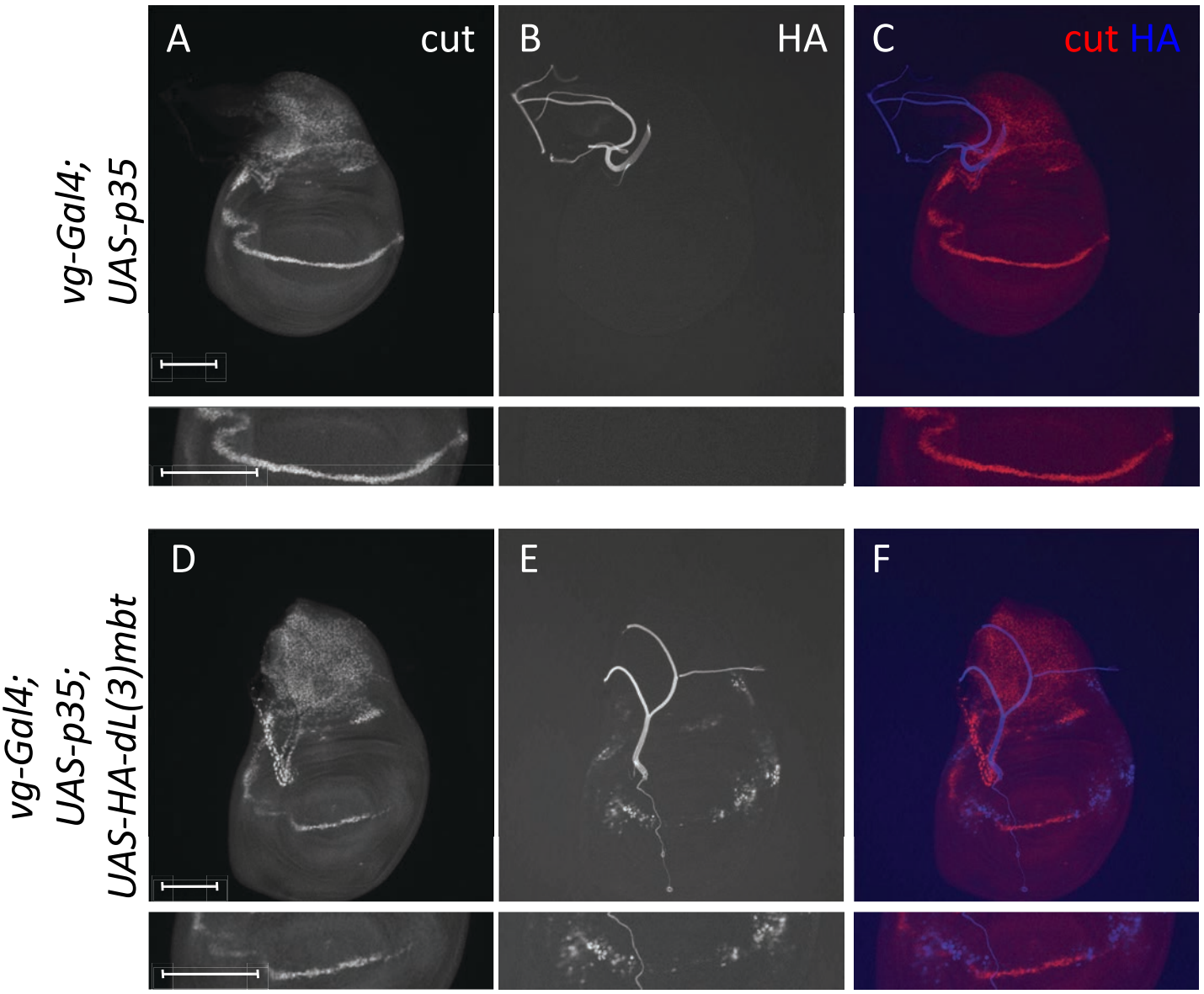

Appendix Figure S11. (Rual)

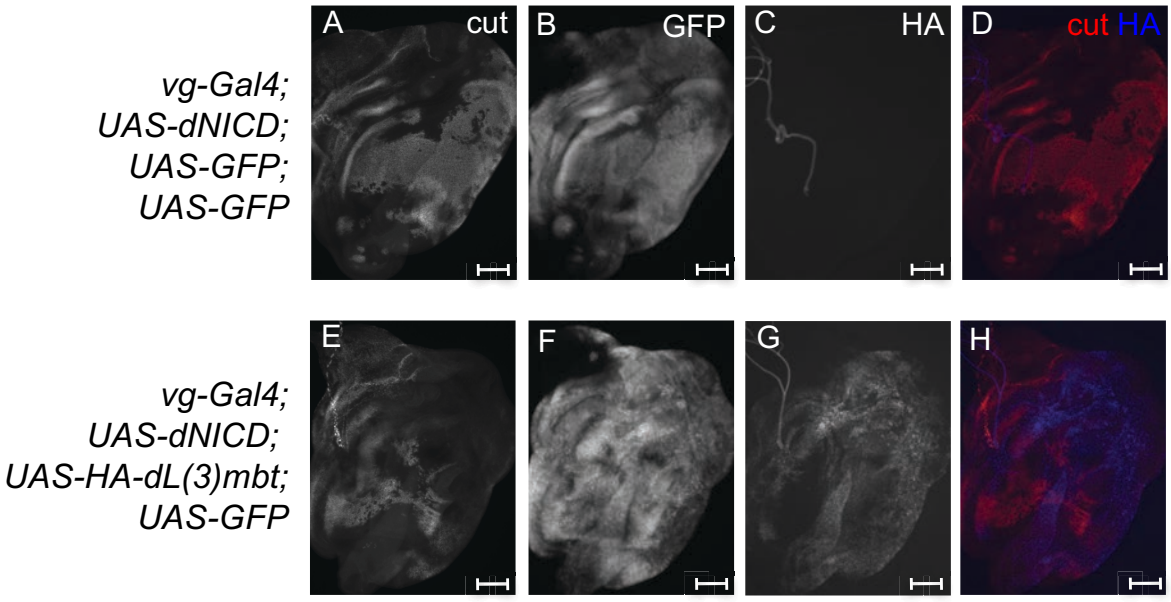

Appendix Figure S12. (Rual)